LATTICE ARRANGEMENTS FOR RAPID CONVERGENCE

Gary R. Hough
Vought Corporation Advanced Technology Center

SUMMARY

A simple, systematic, optimized vortex-lattice approach is developed for application to lifting-surface problems. It affords a significant reduction in computational costs when compared to current methods. Extensive numerical experiments have been carried out on a wide variety of configurations, including wings with camber and single or multiple flaps, as well as high-lift jet-flap systems. Rapid convergence as the number of spanwise or chordwise lattices are increased is assured, along with accurate answers. The results from this model should be useful not only in preliminary aircraft design but also, for example, as input for wake vortex roll-up studies and transonic flow calculations.

INTRODUCTION

The vortex-lattice method (VLM) for the analysis of lifting-surface aerodynamics has become a widely used technique during the past decade. Although originally developed by Falkner in 1943 (ref. 1), it was not until the introduction of high-speed digital computers in the early 1960's that the method was reconsidered and extended, particularly by Rubbert (ref. 2). Since then, many applications of the VLM have been made to problems of aerodynamic design and analysis with considerable success.

The VLM represents a type of finite-element solution to lifting-surface theory problems. As opposed to the alternate kernel-function approach, it "seem(s) to possess none of the traditional values other than some approximation to the calculus of infinitesimals" (ref. 3). Nevertheless, a number of comparisons between the two methods have been favorable overall.

Criticisms of the VLM have continued though. These usually contend either that the lattices can be laid out in a preconceived manner to give some desired answer or that too many lattices are required for adequate convergence of the computed loadings. The present study was undertaken to derive systematically an optimized vortex-lattice layout which overcomes these objections and can be adapted to a wide variety of configurations.

The philosophy of the approach is outlined briefly and then the numerical results are presented.

SYMBOLS

All lengths are dimensionless with respect to the wing root chord.

A	aspect ratio
C_D	induced drag coefficient
C_L	lift coefficient
C_μ	jet momentum coefficient
c	local wing chord
d	tip lattice inset distance, fraction of lattice span
E	flap chord/wing chord
K	vortex drag factor, $\pi AC_D/C_L^2$
M	number of chordwise vortices
N	number of spanwise vortices on wing semispan
T	total number of vortices
x,y,z	right-handed Cartesian coordinates
x_{cp}	x-center of pressure
y_t	wing semispan
α	angle of attack, degrees
β	flap deflection angle, degrees
η	spanwise variable, y/y_t
τ	jet deflection angle, degrees

THE VORTEX-LATTICE APPROACH

The results presented here are based on the commonly used linearized analysis of thin lifting surfaces. The flow is considered to be steady, inviscid, and incompressible (although this latter assumption can readily be relaxed by using the Gothert transformation). While this strictly limits the study to attached flows with small deflections, the basic model has proved its usefulness in many extended applications because of its simplicity and the general agreement with experimental data.

The typical mechanics of the lattice layout, the mathematical details, and the computations of the resulting loads will not be discussed here, as they are assumed familiar or can be found in other reports (e.g., refs. 2,4,5). Rather, the focus of the analysis will be on deriving the optimized lattice structure which results in an accurate, cost-efficient approach to performance prediction for a wide variety of configurations, including wings with flaps and jet-flap systems.

Before proceeding with the details of the optimized VLM, a word about the "accuracy" (or lack of it) of these finite-element approaches is in order. It should be remembered that with the assumptions employed, we are in effect solving a particular boundary-value problem, and a unique solution exists. Hence, all properly formulated finite-element analyses (or assumed loading-function approaches) based on this model should give results which converge to this solution as the number of unknowns is increased indefinitely. There are of course some differences in the ease of application and computational effort involved in the various approaches, but what ultimately distinguishes their merits is how rapidly the results converge to the correct answer. This should be explored numerically for a number of configurations in order to give the ultimate user some degree of confidence in the particular prediction technique.

Since no exact solutions exist (except for the circular wing), determination of just what is the "correct" answer rests entirely upon comparison between two or more different theoretical approaches to the same problem. Thus, in this sense, a favorable comparison of analytical results with particular experimental data does not guarantee that the method is "accurate". Rather, once some degree of accuracy is established through numerical experimentation and agreement with other analyses, comparison with experiment should be used to verify the range of validity of the linearized thin-wing theory model. In cases where agreement is not good, it indicates that a better basic model is required.

NUMERICAL RESULTS

Rectangular Planforms

We first consider the case of an uncambered rectangular wing at angle of attack α, which will serve to illustrate some of the optimized lattice features. A right-handed xyz-coordinate system is chosen such that x is positive in the freestream direction and the origin is located at the wing root leading edge. For convenience, the wing root chord is normalized to unity, that is, all lengths are dimensionless with respect to the root chord. Then this wing geometry is completely described by y_t, the y-coordinate of the wing tip (or equivalently by the aspect ratio A).

The conventional lattice layout for this case (ref. 5) is to use uniformly spaced chordwise and spanwise panels which cover the whole wing. While the computed loads converge, they do so somewhat slowly with respect to the number of spanwise vortices. However, this can be accelerated by employing equally spaced lattices which are inset from the tip by a fraction d of the lattice span ($0 \leq d < 1$). (See fig. 1.) Such an idea was first suggested in reference 7 and was subsequently shown (ref. 6) to afford a marked improvement in spanwise convergence.

This is demonstrated in figure 2 where the percent error in the lift-curve slope per radian CL_α is plotted as a function of the number of vortices on the semispan N for A = 2 and A = 7. The baseline data which are considered to be "exact" for these cases were taken from references 7 and 8, where careful calculations were carried out based on the kernel-function approach. It is seen that the use of d = 1/4 dramatically improves the convergence. In fact, for one

percent accuracy in C_{L_α}, only 5 spanwise vortices need to be used when d = 1/4 as opposed to about 35 when d = 0. Since the computational effort increases as between the square and cube of the number of unknowns, this represents possibly a two order of magnitude cost savings.

A key calculation which further reveals the advantages of spanwise lattice insetting is that of the lift-induced drag. This quantity may be computed by either a near or a far field approach. The latter is based on the work of Munk, in which a Trefftz-plane analysis is used to express the induced-drag coefficient C_D in terms of the Fourier coefficients of the spanwise lift distribution. This has the advantage of relative simplicity (assuming the lift distribution is accurate) but cannot be used to find the spanwise variation of C_D. On the other hand, the near field approach is more demanding of computer time, but does yield this spanwise variation. For the near field computation, we have found it best to use the direct method of summing the forces in the freestream direction on each bound vortex element, neglecting the influence of a bound element on itself. (See also ref. 9.)

In figure 3, the vortex drag factor $K = \pi A C_D / C_L^2$ by both the near and far field methods is shown for the A = 2 wing as a function of N with d = 0 and d = 1/4. The convergence as N is increased is displayed more clearly by plotting K against 1/N. Again, the great improvement in using d = 1/4 is evident, along with the remarkable accuracy of the near field calculation. Further, for no insetting (d = 0), we see that to require very close agreement in the near and far field drags is doomed to failure unless an abnormally large number of spanwise vortices are used. The tendency of the VLM to "predict" low values of K (see ref. 9) is thus shown to be a consequence of not using the optimum lattice inset arrangement.

To illustrate the effect of varying the number of chordwise vortices M, the corresponding variation of K and the x-center of pressure x_{cp} are plotted in figure 4. Note that K is independent of M for M>2 (whether or not insetting is used), while x_{cp} is nearly linear in $1/M^2$ and tip insetting does not improve its convergence rate. For this A = 2 wing, the estimated converged values are $C_{L_\alpha} = 2.474$, $x_{cp} = 0.2094$, and K = 1.001, which are in excellent agreement with those obtained using the kernel-function approach (refs. 7 and 8) of $C_{L_\alpha} = 2.4744$ and $x_{cp} = 0.20939$.

These calculations have been made for an inset distance of one-quarter of a lattice span. A number of tests were made for other values of d, and it is found that d = 1/4 represents approximately the optimum value. As is usual in the VLM, the bound vortices are located at the local lattice quarter chord, and the tangential flow boundary condition satisfied at the local three-quarter chord midway between the trailing vortices. These positions were suggested by two-dimensional results and have been used by Falkner and all who followed. It can be shown that they are mandatory for the three-dimensional case as well (ref. 6).

Several other comments can be made regarding the overall lattice arrangement. First, the use of nonuniform chordwise spacings which bunch the lattices near the leading and/or trailing edges where the variation in vorticity is largest has been investigated. It is found for these uncambered wings that the

uniform chordwise spacing is just as good. Next, various types of nonuniform spanwise spacings (with and without insetting) were also tried, and again the equal span lattice arrangement with d = 1/4 is always superior. Finally, it has been suggested that the results from the VLM will be unreliable when individual lattice aspect ratios drop below a certain value, usually unity. However the calculations here have been carried out using lattice aspect ratios as low as 0.08 with no degredation in accuracy, thus destroying this myth.

Not only the overall loads, but also the spanwise distributions of lift, center of pressure, and induced drag are in excellent agreement with kernel-function results when the optimized layout is used. Regarding computational effort, we find that the execution time rises nearly as the square of the total number of lattices T = MxN up to about T = 80, and then increases to become proportional to N^3 above about T = 120. Calculation of the near field drag increases the basic computational time by approximately 40%. Still, because of the very small number of lattices required (less than 30 for 1/2% convergence in C_{L_α}), computing costs are minimal.

For rectangular planforms, the only parametric study which can be made is on the effect of the aspect ratio A. This was carried out and several interesting features are observed. For example, the induced drag has a maximum at A ≈ 3.5, and the y-center of pressure on the half wing remains very nearly constant. Using a least squares analysis, an attempt to approximate the relationship between C_{L_α} and A along the lines of the classical high and low aspect ratio results yields the formula

$$C_{L_\alpha} = \frac{2\pi A}{A+3} \qquad (1)$$

This is within 1% of the correct value for $16 \geq A \geq 2.5$ and agrees exactly with equation (7-52) of reference 10 for rectangular wings. A somewhat more accurate formula valid down to A = 1 was also found and is shown in figure 5.

Cambered Sections

Since most wing sections have some non-zero camber, it is worthwhile to look at the optimal lattice layout for this case. The study was restricted to rectangular wings with constant spanwise mean lines. However, the conclusions should be applicable to more complicated geometries. Generally, airfoil mean lines are characterized by large negative slopes near the leading edge, and we anticipate that the chordwise lattice spacing is crucial here.

As an example case, an A = 5 wing having an NACA 230 mean line was studied since some results for this case have already been presented (ref. 11). Calculations were made both for the uniform chordwise spacing and for a cosine-type spacing which concentrates the lattices near the leading edge where the change in slope is greatest. The results for C_L are shown in figure 6 as a function of $1/M^2$ for $\alpha = 0°$. It is seen that the cosine spacing converges more rapidly and so is preferable. The estimated converged value is $C_L = 0.077$ which agrees well with the Tulinius result reported in reference 11.

For cambered wings then, it is suggested that a nonuniform chordwise spacing be used for better accuracy. It should be remembered though, that the lift

due to angle of attack will generally be many times larger than the camber contribution and hence errors in computing the camber-induced lift will be somewhat submerged. Thus, for the example case considered at $\alpha = 8°$, the lift due to α is nearly 8 times that due to camber, and the total lift calculated using the uniform chordwise spacing for M = 4 differs by only 1.5% from the cosine spacing result.

Swept Tapered Planforms

The optimized VLM is readily extended to swept tapered wings by insuring that the bound portion of each horseshoe vortex is aligned with the local lattice quarter chord. As the example planform here, we choose the Warren-12 wing, which has been analyzed previously (refs. 7 and 12). It is defined by the x-coordinates of the tip leading and trailing edges of 1.27614 and 1.60947, respectively, and $y_t = 0.94281$. This gives a taper ratio of 1/3 and an aspect ratio of 2.8284. In figure 7 we show the convergence of the lift-curve slope C_{L_α} as a function of 1/N for several values of d. As before, it is seen that d = 1/4 provides about the fastest convergence rate. From this and other planform results, it turns out that the optimum value of d varies slightly with the aspect ratio and sweep angle, but that choosing d = 1/4 is the best compromise for all cases.

The variation of x_{cp} with M and N for this wing is similar to that for rectangular planforms, so that convergence is somewhat slower with respect to M. For the induced drag, both the near and far field calculations were made as before. This time, however, we find that the computed near field drag varies with both M and N, more especially with the former and that K is always less than unity. This poorer drag convergence for swept wings has been noted many times in the past, and arises from the discontinuity in the bound vortex slopes at the wing root. Tulinius (ref. 13) studied this problem and concluded that vortex-lattice approaches which use swept vortices always predict the downwash incorrectly in such regions (or near wing crank locations), but that the error is confined to the immediate neighborhood of the discontinuity. He also showed that the near and far field drag calculations should give identical answers when the bound vortex elements are all parallel.

There is a simple way to improve the near field convergence and accuracy. Suppose we have solved for the local bound vortex strengths using the appropriate swept horseshoe vortex elements. Then, to compute the drag, we must find the sum of the products of the local vortex strengths and the induced downwash at the bound vortex midpoints. Now, though, assume that the downwash is computed using rectangular horseshoe vortices whose strengths are the same as the swept elements which they replace. The results of such a calculation are shown in figure 8 where K is plotted against 1/M and compared with the result using fully swept vortices and also the far field calculation. It is evident that using rectangular elements for the drag calculation only is the answer to the problem. Not only is the dependence on M eliminated, but as it turns out, also the dependence on N. Further, the far field calculations for increasing N converge to this near field value.

While this approach has given a stable answer for the total induced drag, there is still some room for improvement in the convergence of the spanwise drag distribution, $cC_d/\bar{c}C_D$ (where C_d is the local drag coefficient and $\bar{c}$ is the

average chord). As shown in figure 9, the regions near the root and tip converge more slowly, and further study of this problem is needed. It is interesting to note that there is very little difference in the spanwise drag distribution curves for computations made with the rectangular or the swept vortex elements.

The kernel-function approaches also encounter similar difficulties for swept wings. In those analyses, the concept of artificial rounding at the root is often introduced, but only partially alleviates the problems (refs. 7 and 12).

The estimated converged values for this Warren-12 wing are $C_{L_\alpha} = 2.74$, $x_{cp} = 0.751$, and $K = 1.008$. The corresponding results from reference 7 are $C_{L_\alpha} = 2.75$ and $x_{cp} = 0.753$, while from reference 12, $C_{L_\alpha} = 2.74$ and $K = 1.010$. Again, the agreement is excellent. Here too, only a few lattices are required for accurate answers, e.g., a total of 30 lattices gives better than 1/2% agreement with the converged result.

This optimized layout has been used to study the properties of a number of different combinations of sweep and taper, including delta planforms. In all cases, rapid convergence and accurate results were obtained.

Other Planforms

A number of other wing planform arrangements have been studied to give further guidelines for the optimized lattice structure. Consider for example a cranked wing which has one or more discontinuities in the leading or trailing edge sweep angles. Here it is of interest to examine how the spanwise lattices should be laid out since in only a few very special cases will it be possible to use equally spaced lattices across the whole wing and keep $d = 1/4$. As a test case, a planform having both leading and trailing edge cranks located at the midspan ($0.5\ y_t$) with $A = 3.478$ was chosen. Then N_1 vortices were used inboard of the crank and N_2 outboard. The tip inset was set at 1/4 of the outboard lattice span. Figure 10 shows the convergence of C_{L_α} with $1/N$, ($N = N_1 + N_2$), for $N_1 = 0.5N_2$, $N_1 = N_2$, and $N_1 = 2N_2$. Although all three arrangements appear to be converging to the same value, the fastest rate is realized with $N_1 = N_2$ or approximately equal inboard and outboard lattice spans.

Computations with other cranked wings have confirmed this finding; hence, N_1 and N_2 should be chosen to give as nearly equal lattice spans across the wing as possible. This rule is readily extended to wings with more then one spanwise crank location. Also, the induced drag should be calculated using the replacement rectangular vortices.

Other configurations which have been treated include skewed wings and planar interfering surfaces. In the former case, the symmetry with respect to y is destroyed and so the entire wing must be considered rather than just the semispan. While more vortices are required for a given accuracy, the concept of tip insetting with $d = 1/4$ still is needed for rapid convergence. Regarding the planar interfering surfaces, tip insetting is beneficial here also (on both of the wings), but an additional source of trouble is now present. This occurs if one or more trailing vortex lines from the forward surface pass sufficiently close to a control point on the aft surface where the local boundary condition is satisfied. Then, their influence becomes unduly magnified, with irrationa

results. To overcome this instability, it is imperative to select the number of spanwise vortices on each wing carefully so that all the trailing vortices from the forward surface lie approximately on top of the trailing vortices from the aft surface. It is recommended that calculations for several combinations of spanwise vortices be carried out for each case to insure consistent answers.

Wings With Flaps

Although performance predictions for flapped wings using the VLM have received some attention, no detailed convergence studies are available. Indeed, from the results reported to date, it appears as if several hundred lattices are necessary to insure reasonable accuracy. The basic difficulty with flapped wings is that the loading is singular at the flap hingeline, and so a large number of chordwise vortices must be used to define the loading adequately in that region. Even the use of nonuniform cosine spacing about the hingeline does not improve the slow convergence with respect to M.

An optimized lattice arrangement has been developed which considerably reduces the number of unknowns required. For convenience in demonstrating the lattice layout, consider the simple case of a rectangular wing with a full-span trailing edge flap. The flap chord is taken as constant and equal to E, and the flap has a deflection angle β. As usual, the convergence with respect to N is accelerated by tip lattice insetting with d = 1/4. For the chordwise arrangement, we place bound vortex elements directly on the hingeline itself. This was apparently first proposed by Rubbert (ref. 2) but has not been widely used, possibly because few details or numerical results showing its benefits were given. As a result of placing bound vorticity on the hingeline, a finite loading is carried there, as opposed to the theoretically infinite value. However, the integrated loading on a non-zero chordwise element about the hingeline is finite in both cases.

The power of this hingeline-vortex approach was demonstrated initially in the two-dimensional case. There, convergence was greatly improved over the conventional approach, and the results are as good as those obtained using the quasi-continuous lifting-surface analysis of Lan (ref. 14). Calculations for the three-dimensional case are shown in figure 11, for a wing with A = 4 and E = 0.4. It is seen that the convergence of the lift-curve slope C_{L_β} is extremely good when vorticity is placed on the hingeline. From these and other computations, we conclude that less than 100 lattices are sufficient to achieve highly accurate results. This represents a substantial savings in computational effort.

Part-span flaps can be analyzed in a similar manner. That is, bound vorticity is placed along the flap hingeline and extended as necessary to the root and/or tip. The practice of insetting the vortices at the flap side edges was also recommended in reference 2, but numerical calculations here have shown that not only the local, but also the overall, loadings are highly sensitive to such an arrangement. Possibly the concept may be worthwhile in that nonlinear treatment, but it should be avoided when using the linearized approach.

This optimized VLM can be extended to treat wings with multiple flaps. These can be arranged in either chordwise or spanwise directions. For the

multiple chordwise flap case, it is necessary to place bound vortex segments on each of the flap hingelines to insure rapid convergence. The performance of leading edge high-lift devices can also be investigated using these layouts.

While there is a scarcity of good numerical results for comparison purposes, one kernel-function calculation should be mentioned. In reference 15, Garner analyzed a swept untapered wing of aspect ratio 4 with a 25% chord flap extending from the 45% spanwise station out to the tip. Using the kernel-function method, he predicted a value of $C_{L_\beta} = 0.758$ and $C_D = 0.179$. With the optimized VLM and 91 unknowns, $C_{L_\beta} = 0.757$ and $C_D = 0.180$. Here, 7 chordwise vortices (5 ahead of the hingeline and 1 behind) and 13 spanwise vortices (6 inboard and 7 on the flap) were employed. Also, the spanwise lift distribution compared very well for this case.

Finally, to show the versatility of this approach, the predicted spanwise lift distribution on a cranked tapered wing (approximating the Convair 990 planform) at 12° angle of attack with multiple spanwise flaps is plotted in figure 12. Here the seven flaps were deflected through various angles as shown in an attempt to produce a nearly linear dropoff in the loading over the outer half of the wing. Such loadings are of interest in wake vortex roll-up calculations.

Jet-Flap Wings

The optimized VLM has also been applied to predict jet-flap wing performance. The jet flap is basically an arrangement for integrating the propulsion system of an aircraft with its lift production by blowing a narrow jet of high-velocity air from a slot at the wing trailing edge. This deflected jet, besides supplying thrust, also increases the lift through an additional induced circulation as well as by a reaction to its vertical momentum. The additional circulation, or supercirculation as it is sometimes called, arises from the asymmetry induced in the main stream by the presence of the jet and can amount to a large fraction of the total lift on the wing under certain conditions.

Within the linearized theory framework, the trailing jet sheet can be represented by vortex lattices and the appropriate dynamic boundary condition satisfied at corresponding control points. We will consider only the so-called "singular blowing" configuration in which the jet leaves at an angle τ with respect to the slope of the camberline at the trailing edge. The jet strength is described by the parameter $C_\mu(y)$, the jet momentum coefficient. The following results are taken from reference 16 wherein a complete performance analysis was carried out. This work was sponsored by NASA ARC under Contract NAS2-8115.

As in the pure flapped wing, the jet-flap loading exhibits a singular behavior. Here, it is at the trailing edge where the streamline deflection changes abruptly. Thus, in analogy with the plain flap case, we try placing bound vorticity along the wing trailing edge. This was again verified to give good convergence characteristics in the limiting two-dimensional problem. In addition, it turns out to be necessary to use a nonuniform chordwise spacing which concentrates the lattices near the trailing edge. This does have the advantage that the infinite downstream extent of the jet sheet can be mapped into a finite region.

In figure 13, the convergence behavior of the lift-curve slope C_{L_τ} is plotted for full-span blowing from a rectangular wing with A = 2 and C_μ = 1. The superiority of placing bound vorticity at the trailing edge is clear. Note that the lift on the wing is computed by adding the jet reaction component to the wing bound vortex, or circulation, lift. The numerical experiments indicate it is best to consider all of the trailing edge vortex lift applied to the wing, as shown in the figure. Overall, we must use a somewhat larger number of chordwise vortices for the jet flap, but again the total number required is considerably smaller than used in previous studies.

For the above wing, the estimated converged values are C_{L_τ} = 2.00 and x_{cp} = 0.816. These can be compared with the results obtained in reference 17 by using an adaptation of Lawrence's improved low aspect ratio approximation, where it was calculated that C_{L_τ} = 2.01 and x_{cp} = 0.810. Comparable agreement was found at other values of A and C_μ for these rectangular planforms.

Other planforms and blowing arrangements have also been treated. Thus, part-span blowing was analyzed and y-variations in C_μ (nonuniform blowing) were taken into account. An example calculation for nonuniform blowing over part of the wing span is illustrated in figure 14. In this case, the jet extended from the 25% to the 75% spanwise station, and C_μ varied quadratically in this region.

An interesting result of the nonuniform blowing calculations is that the wing circulation lift as well as its spanwise distribution is relatively unaffected by varying C_μ provided that the total, or integrated, jet momentum coefficient is the same for both cases. Thus, we can conclude that for most practical purposes, it will be sufficient to carry out nonuniform blowing calculations for the corresponding uniform blowing case with the same total jet coefficient, and then add in the true nonuniform jet reaction components to find the total lift, center of pressure, etc., at each spanwise location.

CONCLUSIONS

In conclusion, a simple, systematic optimized vortex-lattice layout has been developed for application to a wide variety of configurations. It results in a significant reduction in computational costs when compared to current methods. The key elements are:

(a) Use of tip lattice insetting to accelerate convergence as the number of spanwise lattices is increased.
(b) Placement of bound vortices at locations where discontinuities in streamline slope occur (flap hingeline, jet-flap trailing edge) to accelerate convergence as the number of chordwise vortices is increased.
(c) Use of nonuniform chordwise spacing for cambered sections and jet-flap wings to accelerate convergence for these cases.
(d) Use of rectangular horseshoe vortices to compute the near field drag.

Rapid convergence as the number of spanwise or chordwise lattices are increased is assured, along with accurate answers. The results from this model should be useful not only in preliminary aircraft design but also, for example, as input for wake vortex roll-up studies and transonic flow calculations.

REFERENCES

1. Falkner, V. M.: The Calculation of Aerodynamic Loading on Surfaces of Any Shape. Great Britain, ARC R&M 1910, August 1943.

2. Rubbert, P. E.: Theoretical Characteristics of Arbitrary Wings by a Non-planar Vortex Lattice Method. Boeing Co. Report D6-9244, 1964.

3. Ashley, H.; and Rodden, W. P.: Wing-Body Aerodynamic Interaction. Annual Review of Fluid Mechanics, Vol. 4, 1972, pp. 431-472.

4. Giesing, J. P.; Kalman, T. P.; and Rodden, W. P.: Subsonic Steady and Oscillatory Aerodynamics for Multiple Interfering Wings and Bodies. J. Aircraft, Vol. 9, No. 10, 1972, pp. 693-702.

5. Margason, R. J.; and Lamar, J. E.: Vortex-Lattice Fortran Program for Estimating Subsonic Aerodynamic Characteristics of Complex Planforms. NASA TN D-6142, February 1971.

6. Hough, G. R.: Remarks on Vortex-Lattice Methods. J. Aircraft, Vol. 10, No. 5, 1973, pp. 314-317.

7. Medan, R. T.: Improvements to the Kernel-Function Method of Steady, Subsonic Lifting Surface Theory. NASA TM X-62,327, March 1974.

8. Labrujere, Th. E.; and Zandbergen, P. J.: On the Application of a New Version of Lifting Surface Theory to Non-Slender and Kinked Wings. J. Engineering Mathematics, Vol. 7, No. 1, 1973, pp. 85-96.

9. Kalman, T. P.; Giesing, J. P.; and Rodden, W. P.: Spanwise Distribution of Induced Drag in Subsonic Flow by the Vortex Lattice Method. J. Aircraft, Vol. 7, No. 6, 1970, pp. 574-576.

10. Jones, R. T.; and Cohen, D.: High Speed Wing Theory. Princeton University Press, 1960.

11. Wang, H. T.: Comprehensive Evaluation of Six Thin-Wing Lifting-Surface Computer Programs. NSRDC Report No. 4333, June 1974.

12. Garner, H. C.; Hewitt, B. L.; and Labrujere, Th. E.: Comparison of Three Methods for the Evaluation of Subsonic Lifting-Surface Theory. Great Britain, ARC R&M 3597, June 1968.

13. Tulinius, J.: Theoretical Prediction of Airplane Stability Derivatives at Subcritical Speeds. North American Rockwell Co. Report NA-72-803, 1972.

14. Lan, C. E.: A Quasi-Vortex-Lattice Method in Thin Wing Theory. J. Aircraft, Vol. 11, No. 9, 1974, pp. 518-527.

15. Garner, H. C.: The Vortex Drag of a Swept Wing with Part-Span Flaps. Great Britain, ARC R&M 3695, September 1970.

16. Hough, G. R.: Aerodynamic Performance of Jet-Flap Wings. NASA CR-137858, February 1976.

17. Erickson, J. C.; and Kaskel, A. L.: Theoretical Solutions and Numerical Results for Low-Aspect-Ratio Rectangular Jet-Flap Control Surfaces. Therm Advanced Research Report TAR-TR 6603, December 1966.

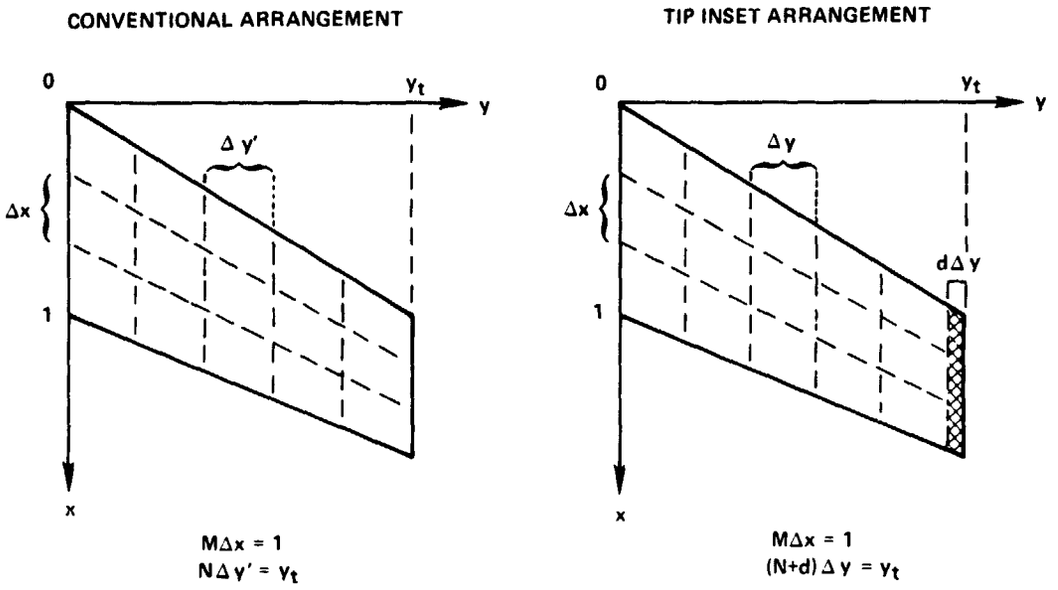

Figure 1.- Vortex-lattice layout.

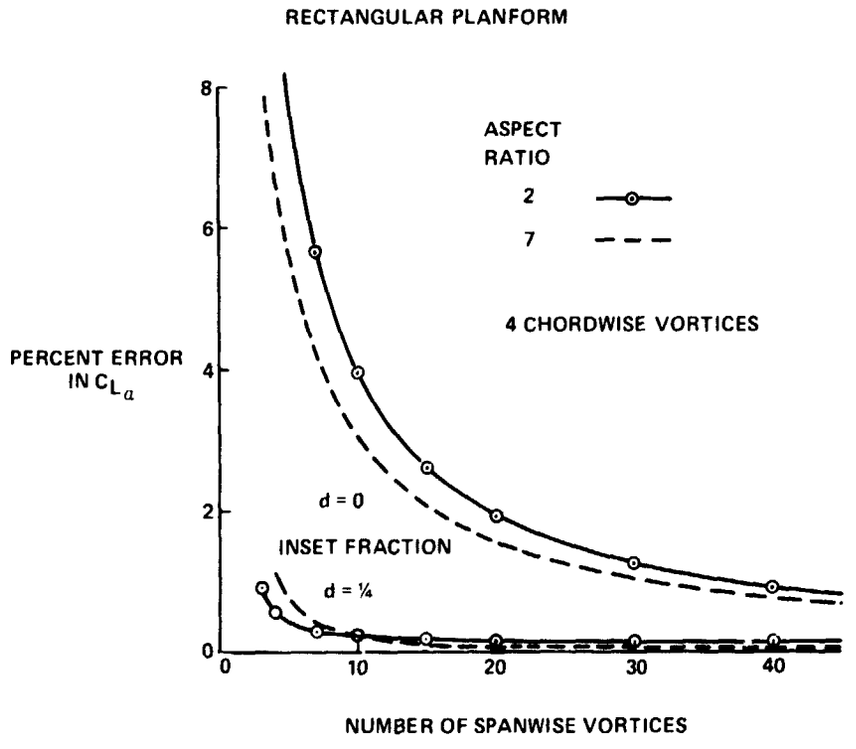

Figure 2.- Lift-curve slope convergence for rectangular wing.

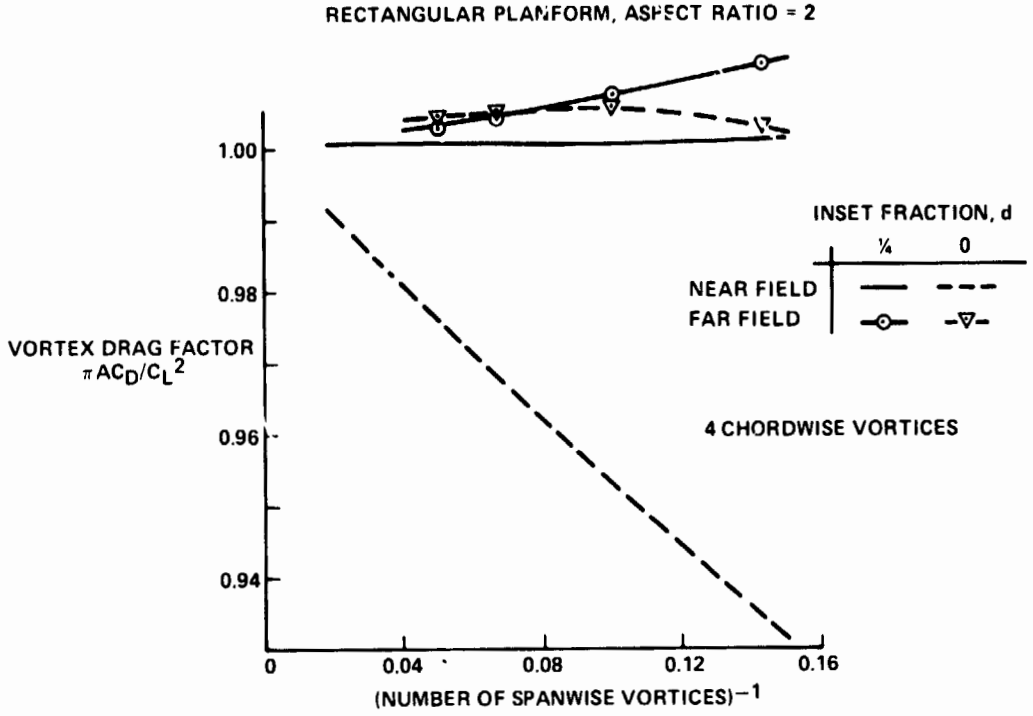

Figure 3.- Comparison of near and far field induced drag.

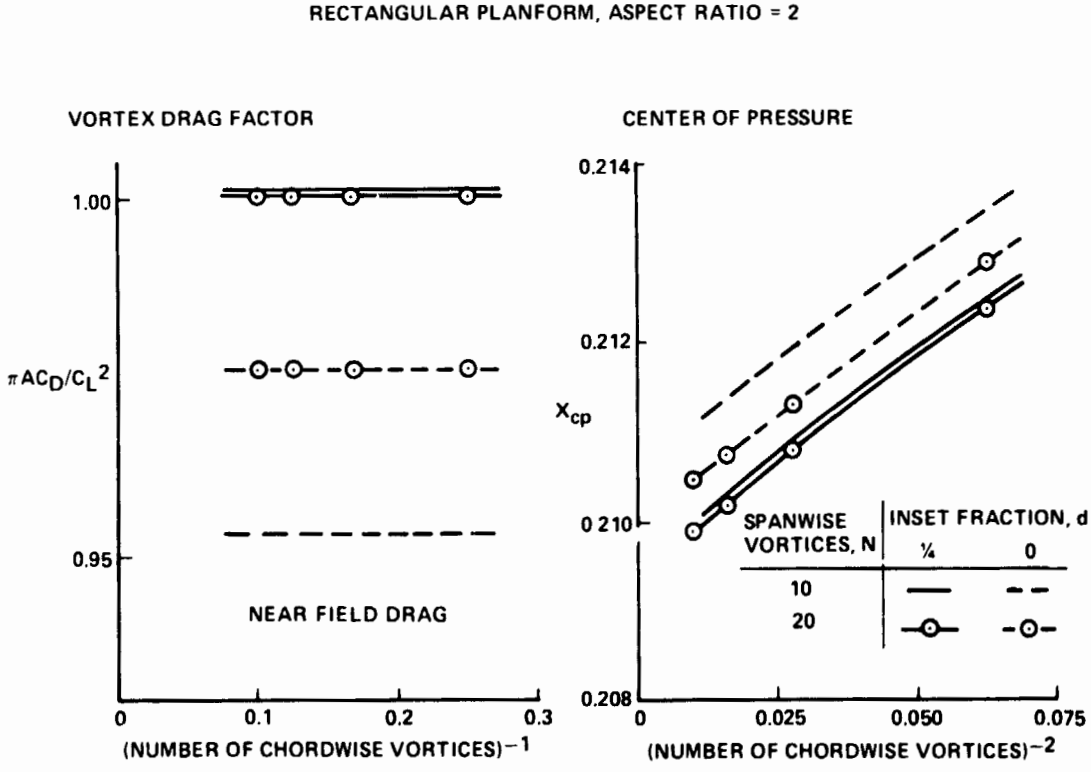

Figure 4.- Convergence behavior for rectangular wing.

- LIFTING-LINE THEORY (PRANDTL) – HIGH ASPECT RATIO, ELLIPTIC PLANFORM

$$C_{L_\alpha} = \frac{2\pi A}{A+2}$$

- LOW ASPECT RATIO THEORY (JONES)

$$C_{L_\alpha} = \frac{2\pi A}{A+4}$$

- NUMERICAL LIFTING-SURFACE THEORY (HOUGH) – RECTANGULAR PLANFORM

a. $C_{L_\alpha} = \frac{2\pi A}{A+3}$ (1% ACCURACY FOR $16 \geq A \geq 2.5$)

b. $C_{L_\alpha} = \frac{2\pi A}{A+2.903+\frac{0.377}{A}}$ (3/4% ACCURACY FOR $16 \geq A \geq 1$)

Figure 5.- Lift-curve slope formulas.

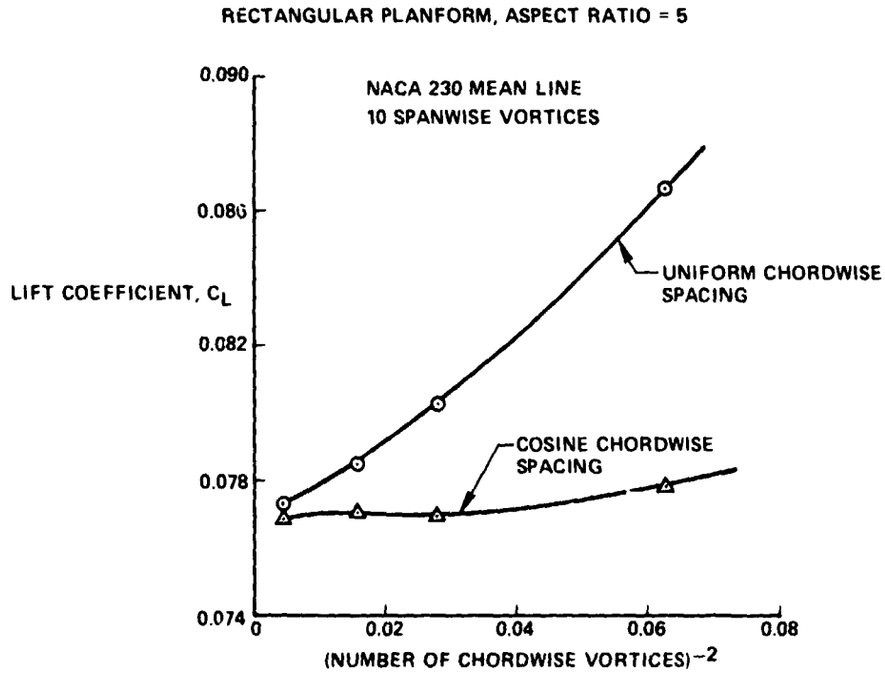

Figure 6.- Convergence for cambered wing.

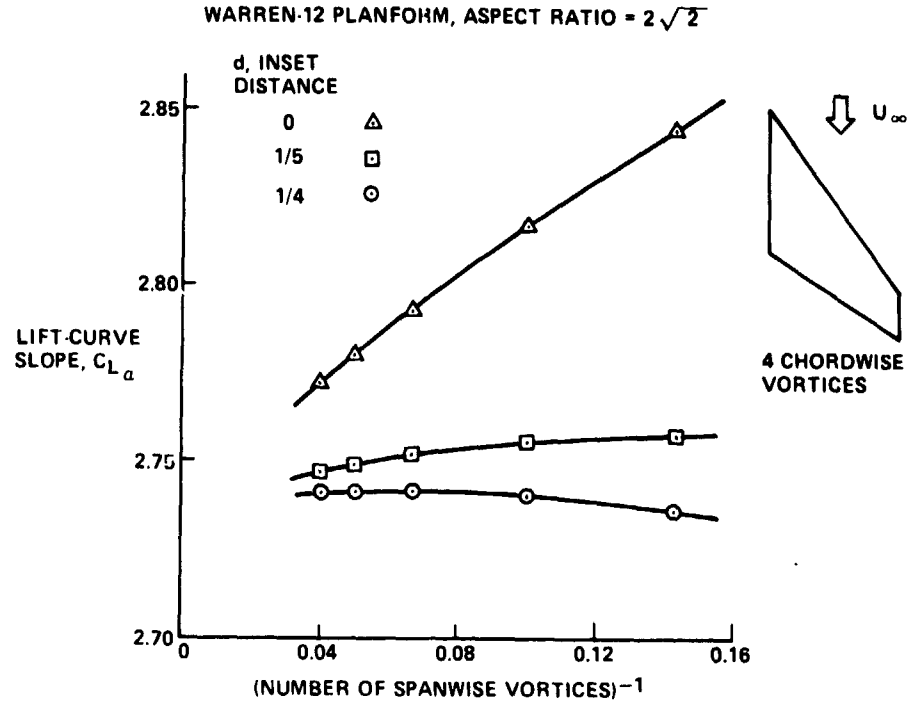

Figure 7.- Lift-curve slope convergence for tapered wing.

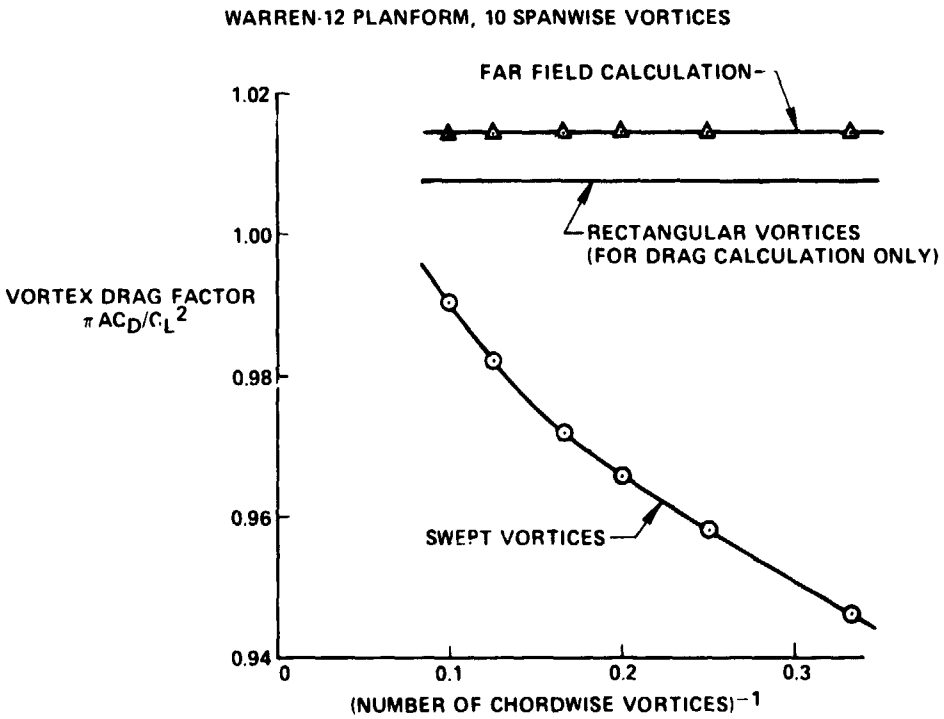

Figure 8.- Induced drag for tapered wing.

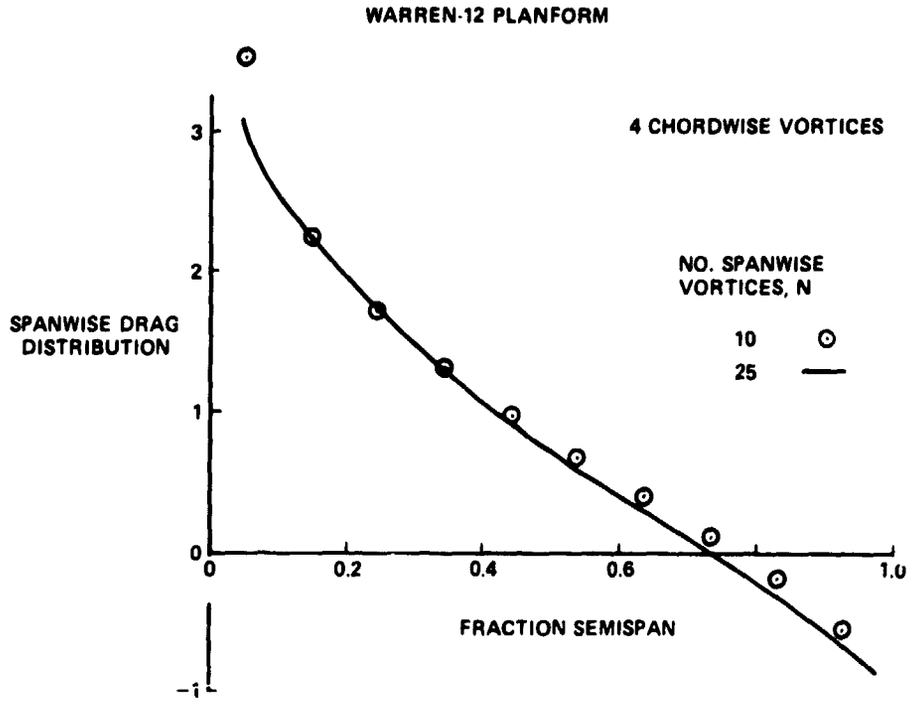

Figure 9.- Spanwise drag distribution for tapered win.

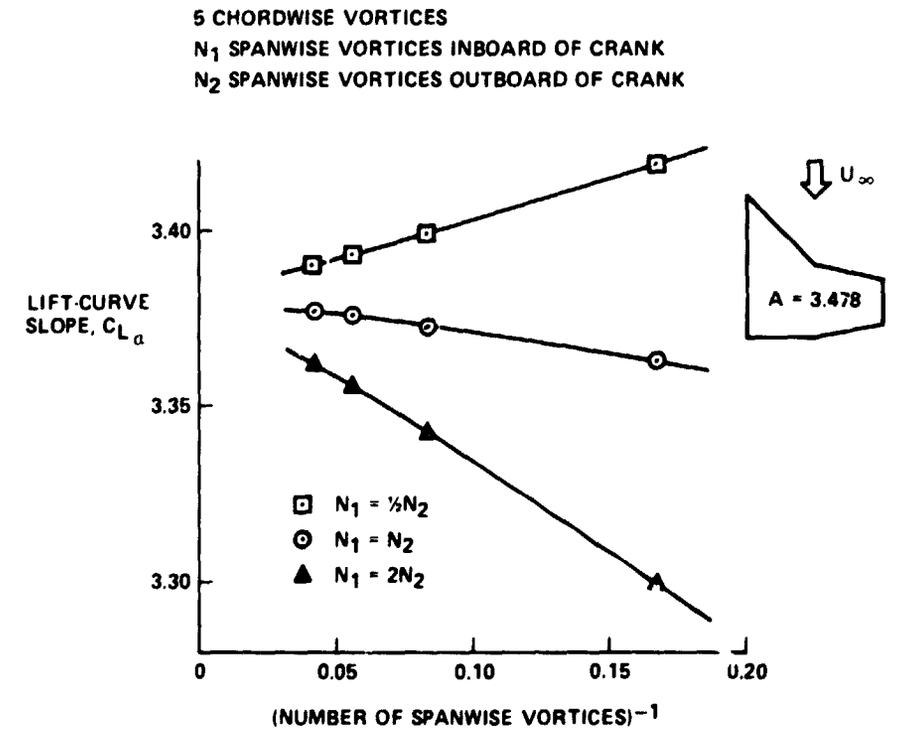

Figure 10.- Lift-curve slope convergence for cranked wing.

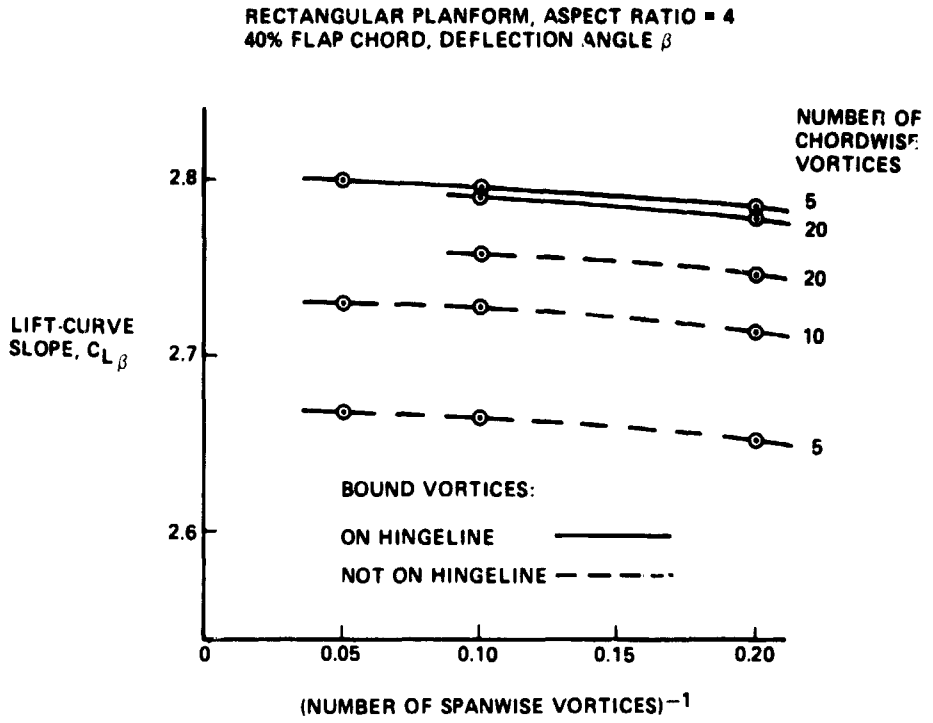

Figure 11.- Lift-curve slope convergence for flapped wing.

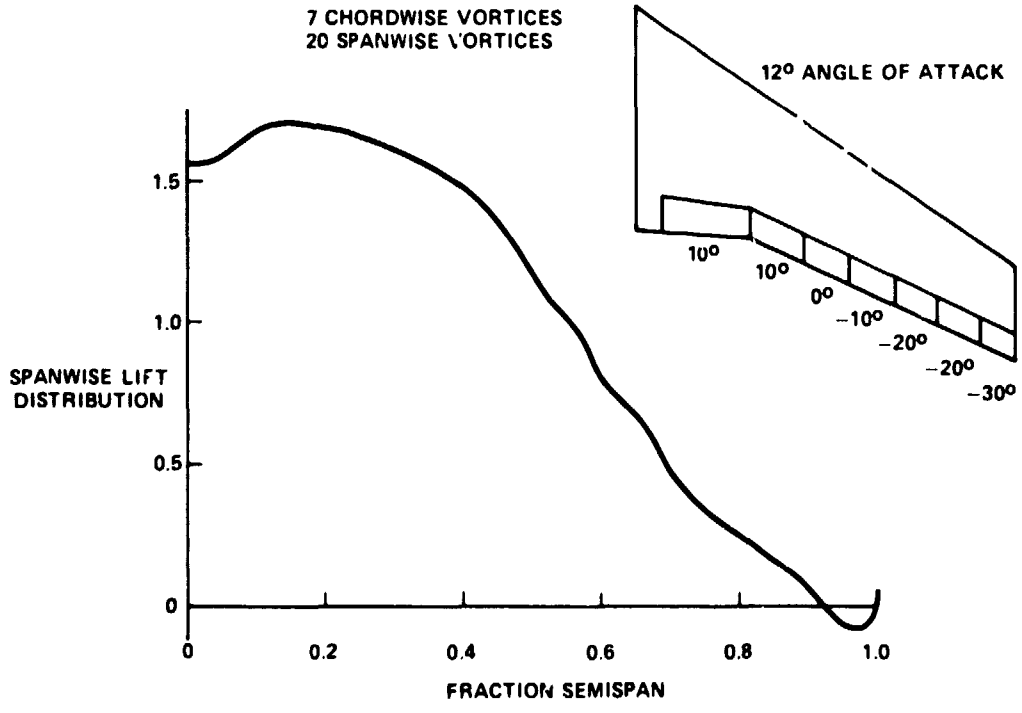

Figure 12.- Spanwise lift distribution for multiple flap configuration.

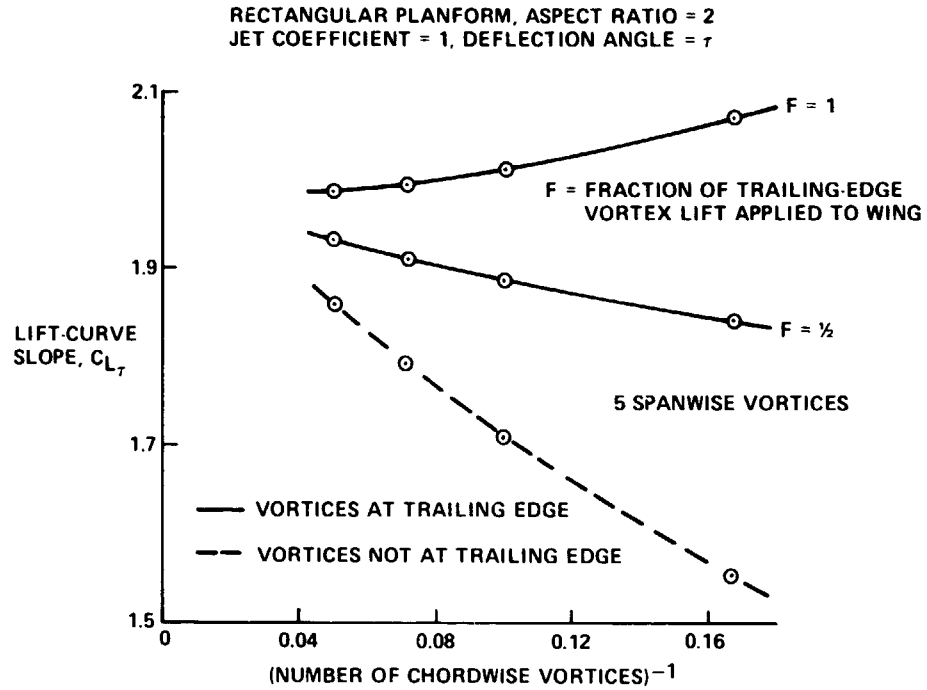

Figure 13.- Lift-curve slope convergence for jet-flap wing.

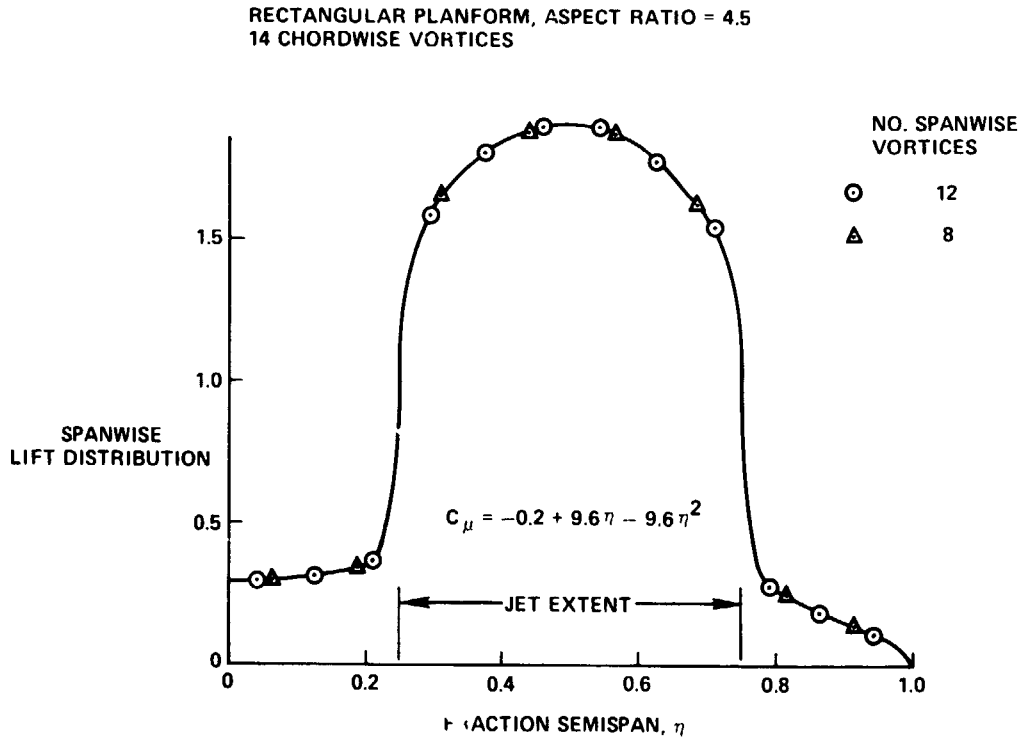

Figure 14.- Spanwise lift distribution for nonuniform blown, part-span jet flap.